Research Article

Jiameng Wu, Benqiang Lou, Jiaxia Wang, and Kun Liu*

Experimental investigation and numerical analysis of stress concentration distribution at the typical slots for stiffeners

Abstract: Stress concentrations typically exist around the perimeter of an opening and on attached structures, thereby resulting in a potential risk of crack initiation. Experimental and numerical methods on stress concentration distribution analysis can be applied in this study. This study reveals the differences in stress concentration distributions around various types of slots. Typical slots have been selected to discuss the influence on stress concentration distribution when the connections of flat bar and connection plate are considered. This concept is novel given the experiments conducted and finite element method (FEM) results found under complex loads. The FEM is used to compare calculated results with experimental data, and continuous plotting of numerical results can verify the outcomes. The results show the stress concentration distribution around the selected slot edge, where peak stress appears around the openings of different types of slots.

Keywords: ship structures, typical slots, stress concentration, opening strengthening, model test, numerical simulation

1 Introduction

Some survey data show that 70% of structural damage in ships is caused by local stress concentration. The summary of the Ship Structure Committee (SSC) (1990) emphasized that fatigue damages are crucial, especially for vessels exceeding 200 m in size. With a large-scale trend in ship construction, local structure failures have received increasing attention due to stress concentrations. In ship structures, when stiffeners traverse the web of primary supporting members, cutouts or slots for stiffeners and the related collaring arrangement (including collar plate [CP] and/or web stiffener) are designed to minimize stress concentrations around the perimeter of the opening and on the attached web stiffeners (if arranged), where angled elliptical slots must be laid during construction, as illustrated in Figure 1.

Moreover, Figure 2 depicts that irregular stress will appear at the local construction of the elliptical slots considering the pressure differences between the interior and exterior of a side or a bottom shell. Understanding the stress concentration distribution around the opening is necessary to harmonize stress distribution during the design of local slots [1].

Various methods, such as elasticity theory, computational techniques, and experimental stress analysis, are available for evaluating stress concentrations in plates given geometrical irregularities in openings (or cracks). For an analytical solution, the early work of Muskhelishvili discussed the complex variable approach to stress analysis considering the elliptical cavity under uniform loading and elasticity theory [2]. When a conformal mapping function is relative to the example of elliptical or regular polygonal holes with rounded corners and for additional complex geometries, the method used becomes semi-analytical, and numerical methods are used to obtain coefficients of power series expansion [3–7]. The method obtains a well-designed closed-form solution for stress concentration around holes, and current practical applications

* Corresponding author: Kun Liu, State Key Laboratory of Ocean Engineering, Shanghai Jiao Tong University, Shanghai 200240, China; Department of Marine Engineering, School of Naval Architecture and Ocean Engineering, Jiangsu University of Science and Technology, Zhenjiang 212003, China, e-mail: kunliu611@163.com
Jiameng Wu: Marine Design & Research Institute of China, Shanghai 200011, China; State Key Laboratory of Ocean Engineering, Shanghai Jiao Tong University, Shanghai 200240, China
Benqiang Lou, Jiaxia Wang: Department of Marine Engineering, School of Naval Architecture and Ocean Engineering, Jiangsu University of Science and Technology, Zhenjiang 212003, China

Figure 1: Cutouts and slots form on the ship constructions.
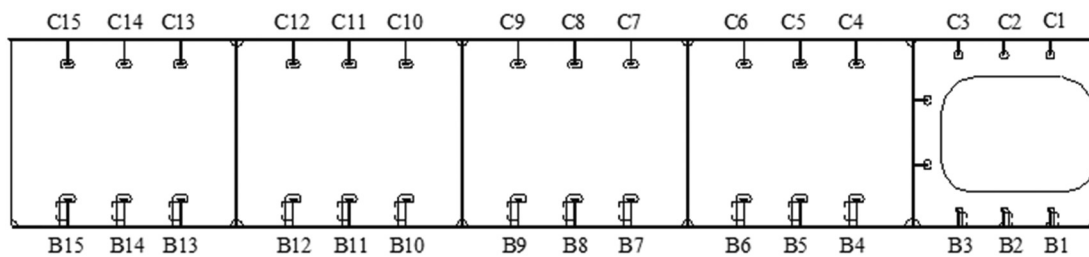

Figure 2: Shape of cutouts or slots in double bottom.

include perforated plates and aircraft and automobile windows. The algorithm for analytical (or semi-analytical) calculation is superior to three-dimensional (3D) ship construction solutions under complex loading and boundary conditions [8,9].

Given the analytical solutions for openings of plates, a method that considers the hole effects on 3D slot structures must be developed. The present study was conducted on the basis of an industrial agreement on the framework of a ship to investigate the stress distribution around an industrial circular or ovaloid hole. Two practical loading conditions, namely, compression on the top plane and bending moments along the specimens, are considered in the test. Few studies have been conducted on the stress concentration of industrial slot constructions. In the 1990s, the Japan Ship Research Association conducted a model test of the connection structure between the longitudinal and transverse bulkheads of a ship [10]. Then, Sumi *et al.* used this experimental model as the research object and established the finite element method (FEM) to analyze a ship's side longitudinal connecting structure [11]. The ISSC conducted an experimental study on the connection structure of longitudinal frames and transverse bulkhead of floating production storage and offloading by adopting two equal-scale models. The effects of different cell models and grid sizes were compared with those established by the Classification Society. Lotsberg and Landet designed five test schemes for the connection structure of longitudinal frames and transverse bulkhead of a ship's side. The analysis was compared with numerical results [12]. Wan and Xu conducted another "stress concentration" study on the hole edge based on ABS tanker rules using ANSYS. A table of stress concentration coefficient was presented relative to the various forms of hole openings [13,14].

In fact, the theoretical analysis method can only solve the problem of hole edge stress distribution of regular holes such as circle, ellipse, and rectangle, while the actual hole shape of hull structures is mostly irregular. It is necessary to design and carry out relevant model tests and simulation analyses to determine the hole edge stress distribution, so as to effectively guide the optimization of hole design. This study investigates problems associated with the stress concentration in perforated plates. An analytical solution for stress analysis of metallic plates with central cutouts of various shapes is presented. In addition, numerical studies using commercial finite element software were conducted to evaluate the analytical results. In the present study, the material behavior is assumed to be linearly elastic. Furthermore, the cutout

is small, its effect will be negligible at a distance of a few diameters from its edge, and points at such distance may be regarded as at infinity.

In the present study, a shipyard has recognized three main types of slots (i.e., NT2, T1, and YB1) for stress measurements, wherein the finite element tool ABAQUS was used to describe the stress distribution trends. A total of 48 specimens have been tested in this study for specific loading cases. By comparing numerical results with experimental data, the matched FE results have been verified for the selected typical forms. Based on the results, the influence of hole shapes and reinforcements on product performance was discussed, and guidance on local optimization was provided [11,15].

2 Description of the specimen and loading conditions

2.1 Materials

The material used during the experiment is mild steel that contains 0.15–0.23% carbons with a Young's modulus of 2.10 GPa and a density of 7,850 kg/m^3. The yield stress is 235 MPa, and the welding influences and small defects on the hole are disregarded during the construction of the slots. Deformations remain under the assumption of elasticity during the test [16].

2.2 Geometry of the test specimen

The related experimental specimens have been obtained from double bottom hull structures approved by the shipyard. A comparative analysis has been performed on six kinds of test models, namely, NT2-CP0-FB0, NT2-CP1-FB0, NT2-CP0-FB1, NT2-CP1-FB1, T1-CP0-FB0, and YB1-CP0-FB0. The analysis has considered the influence of the cutout types and reinforcement forms. Different comparisons have been conducted on the basis of the different slot types (i.e., NT2, T1, and CP0; Figure 3), cutout location with or without CP, and web stiffener of a FB.

To fully understand the effect of a patch or stiffener, the six experimental models are catalogued with different stress distributions around the cutouts, wherein NT2, T1, and YB1 reflected the slot types; the CP and FB represent the test specimen with (1) or without (0) a CP; the FB shows the location connected (1) or not connected (0) by an FB. Table 1 lists the model types.

For convenience, a model of the double bottom structure of the hull has been scaled down for experimentation under laboratory test conditions. The following specific dimensions of the primary test model are presented: the upper and lower panels: 800 mm × 400 mm × 10 mm; horizontal web: 800 mm × 540 mm × 10 mm; T profile: 50 mm × 10/100 mm × 10 mm; CP: 85 mm × 80 mm × 10 mm; and web stiffener of the FB: 300 mm × 100 mm × 10 mm. Figure 4 demonstrates the detailed size parameters of each model [17,18].

3 Experiments

3.1 Description of the experiment

After confirming the test specimen as a model of the ship's double bottom structure, experiments were performed using YNS1000 electrohydraulic servo universal
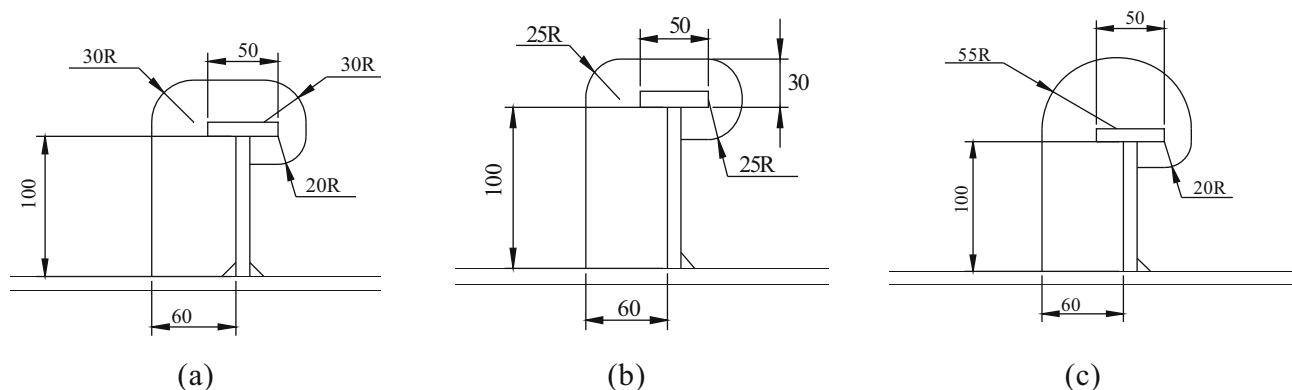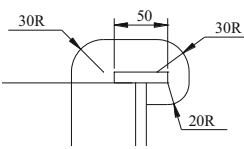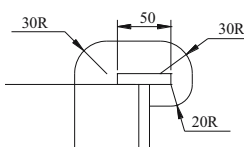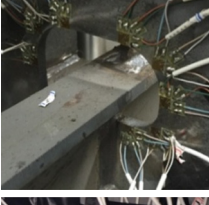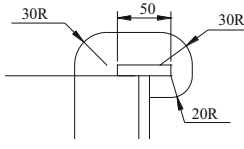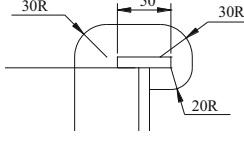

Figure 3: Detailed description of the slot types: (a) NT2, (b) YB1, and (c) T1.

Table 1: Test model types

Specimen types	Paragraph	Slot types (NT2, T1, or YB1)	CP 85 × 80 × 10	Web stiffener 300 × 100 × 10
NT2-CP0-FB0			Without	Without
NT2-CP1-FB0			With	Without
NT2-CP0-FB1			Without	With
NT2-CP1-FB1			With	With
T1-CP0-FB0			Without	Without
YB1-CP0-FB0			Without	Without

test machine, as exhibited in Figure 5. A windows-based microcomputer controls YNS1000 to collect the testing data and draw the curve in real time. Stretch, compress, or shear loadings can be applied through an oil source of the hydraulic pump with the advantages of stable and reliable operations and low noise.
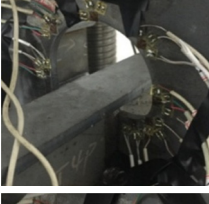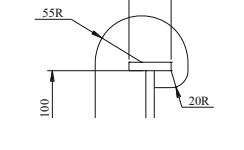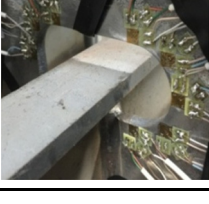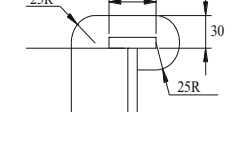
YNS1000 has the advantage of a high-precision durable use, especially fit for the large magnitude load test. The load capacity of this equipment is 1,000 kN with ±0.5%

deformation and displacement measurement accuracy. Table 2 summarizes the characteristics of the machine. The model tests are carried out at room temperature and based on the basic requirements of mechanical experiments with metal materials.

The test specimens are placed on the test platform, and a steel gasket with the same length and width as the upper surface of the model is set on the upper panel to ensure that the loaded load is evenly loaded on the upper surface.
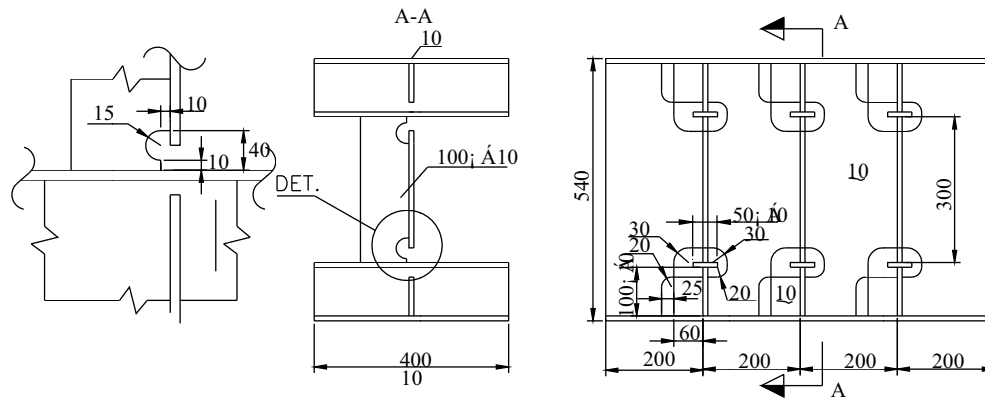
Figure 4: Detailed size diagrams of NT2–CP1–FB1 test specimen (unit, mm).
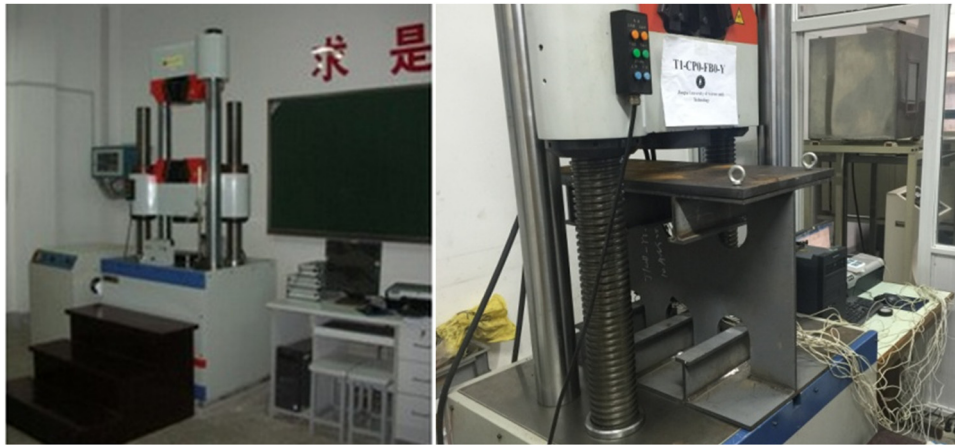

Figure 5: Electro-hydraulic servo universal testing machine, YNS1000.

In the loading process, it is uniformly loaded by the electro-hydraulic servo universal testing machine. Loading and deformation occur in the elastic range (before the test, experiments have been carried out to determine the elastic–plastic range), in which the hierarchical loading control will be adopted before the yielding point is obtained. The target compression forces of 10.0, 20.0, 30.0, and 40.0 t have been applied separately. Figure 6 exhibits the test using YNS1000.

A virtual steel plate is positioned on top of the specimen, and this plate is the same size as that of the specimen top plate. The pressure is transferred to the specimen uniformly through the mechanical arrangement of this virtual plate on the top. The plate is used to simulate water pressure on the side shell condition while considering internal and external differences. The boundary of the specimen will be constrained as a free condition.

Table 2: Characteristics of the equipment

| Model geometry specification		YNS1000
Clamping range (mm)	Cylindrical specimen	Φ10–60
	Plate specimen	0–40
Bending test-bed	Distance between two supports (mm)	50–300
	Max. width of specimen (mm)	160
Distance between two columns (mm)		550
Max. distance between grips (mm) (incl. piston stroke)		700
Max. distance between upper lower compression plate (mm)		500
Dimensions (mm) H.W.D	Mainframe	2,550 × 1,200 × 710
	Hydraulic source	970 × 700 × 850
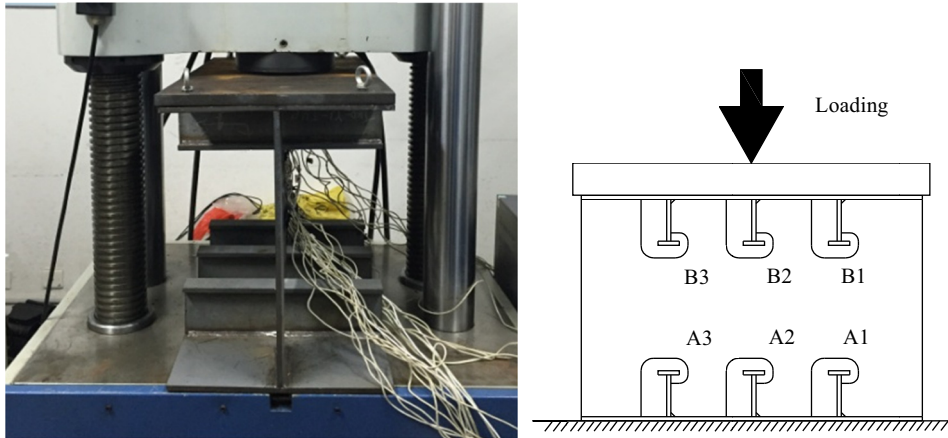
Figure 6: Schematic arrangement of the compression force test.

The same device can be used to measure the stress distribution under a three-point bending loading condition. The results indicate the influences of a structural opening on the local longitudinal strength at the longitudinal frames or the bottom connections. Figure 7 displays that the line concentrated force will apply to the mid-position of the top surface, and the bottom of the specimen will be constrained with the displacement at the connection ends of A1 and A3 given a distance of 400 mm. Concentrated force is applied in sequence with the magnitudes of 1.0, 2.0, 3.0, and 4.0 t. Then, the bending moment is generated along the side edge in the longitudinal direction.

Therefore, six kinds of specimens are tested. Moreover, two loading conditions and four loading steps of each loading condition are applied for each specimen. To further verify the results, approximately 70 special cases are considered, including failure cases, during the entire test process.

3.2 Stress measurements

A uniform experimental approach was adopted in the test on the basis of the strain measurement around the hole. The distance was measured in millimeters using miniature strain gauges next to the edge of the hole. Then, the local stress distributions were considered by using strain measurement, particularly for complex geometrical components.

Before strain measurement, numerical calculations were conducted to describe the concentrated stress around the hole in the initial stage. Figure 8 presents the strain gauge layout based on the stress distribution results. Nine strain measuring points (i.e., A, B … I) were available around the hole for the NT2 type. Positions B, D, and G were determined for −30°, 20°, and 160° at the position of a quarter cycle. Measurement locations A, E, and F were positioned at the perimeter of a cycle and a flat cut considering the angles of −20°, 60°, and 120°. Points C and H

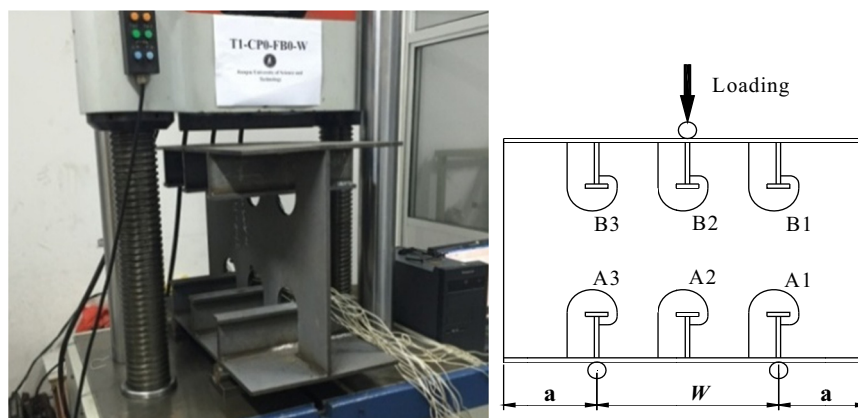**Figure 7:** Schematic arrangement of the bending test.

(a) (b) (c)

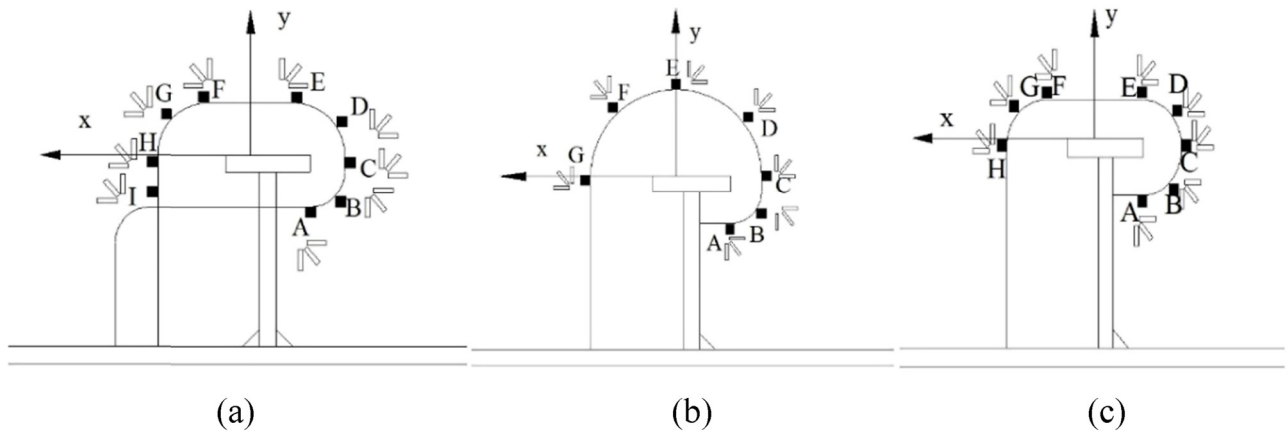**Figure 8:** Illustration of strain gauge layout with slot types: gauge layout of (a) NT2 (with CP), (b) T1, and (c) YB1.
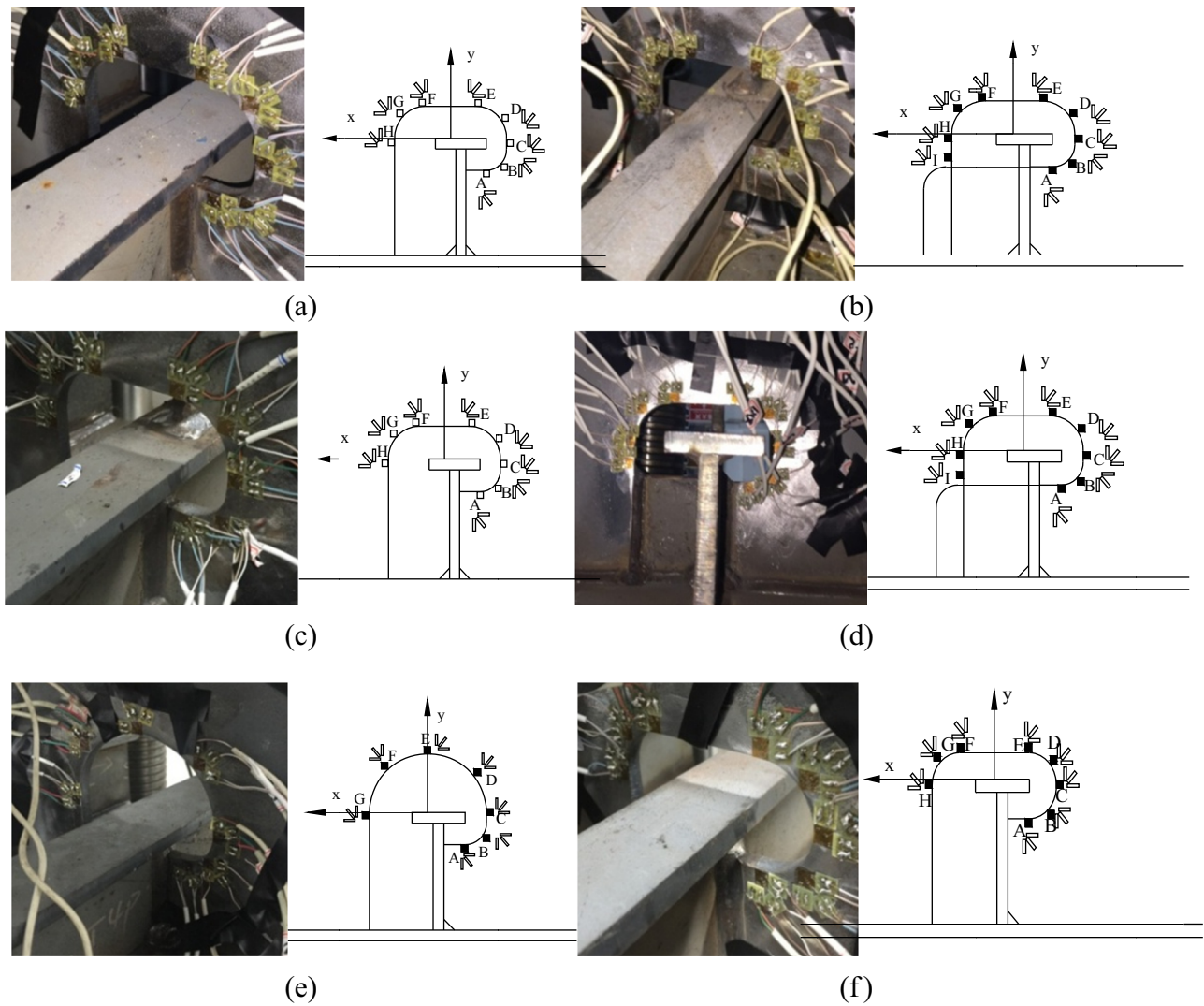

(a) (b)

(c) (d)

(e) (f)

Figure 9: Measuring point arrangement of real experimental component. (a) NT2-CP0-FB0, (b) NT2-CP1-FB0, (c) NT2-CP0-FB1, (d) NT2-CP1-FB1, (e) T1-CP0-FB0, and (f) YB1-CP0-FB0.

Table 3: Stress results at the locations under compression conditions of B2 (unit: MPa)

		A	B	C	D	E	F	G	H	I
NT2-CP0-FB0	10T	37.04	39.29	40.93	13.18	—	11.65	33.34	—	—
	20T	129.13	158.23	140	30.93	—	50.18	65.15	—	—
	30T	207.77	219.52	218.02	63.36	—	58.25	91.81	—	—
	40T	315.17	333.63	324.43	95.98	—	49.78	100	—	—
NT2-CP1-FB0	10T	34.65	43.95	75.97	67.91	11.33	12.11	16.53	61.2	—
	20T	43.93	55.47	110	97.16	22.88	17.78	54.57	124.57	—
	30T	54.56	80.47	145	125.71	30.8	25.78	79.65	167.7	—
	40T	59.80	120.61	212.65	161.51	0.99	30.16	106	255.25	—
NT2-CP0-FB1	10T	40.1	48.11	9.63	5.42	—	2.18	25.15	29.66	—
	20T	39.6	95.1	42.82	19.83	—	2.51	33.54	52.89	—
	30T	33.41	138.02	73.13	28.38	—	4.1	30.71	77.18	—
	40T	47.53	167.55	108.19	33.36	—	5.3	64.06	103.1	—
NT2-CP1-FB1	10T	78.45	114.93	52.64	68.05	24.25	40.67	55.06	34.86	22.09
	20T	56.08	124.46	94.01	99.85	30.06	55.2	76.91	67.26	40.76
	30T	22.52	154.67	145.86	111.31	27.97	73.87	112.66	91.88	62.8
	40T	54.03	178.32	183	141.46	19.97	113.84	147.95	146.29	88.55
T1-CP0-FB0	10T	79.41	107.88	94.29	59.69	7.59	19.09	37	—	—
	20T	79.56	145	141.49	82.03	12.61	30.63	62.01	—	—
	30T	67.13	169.96	200.97	106.38	15.32	46.53	92.92	—	—
	40T	43.42	188.71	247.91	133.46	17.51	63.3	113.97	——	—
YB1-CP0-FB0	10T	17.7	56.77	86.94	53.89	—	9.97	9.11	21.69	
	20T	30.71	118.88	131.02	102.53	—	10.47	19.2	39.99	
	30T	42.79	181.08	205.1	149.67	—	17.06	26.06	58.91	
	40T	53.1	235.53	246.85	193.9	—	19.23	33.82	79.25	

were placed at the same level as the FB, thus representing the angles of 0° and 180°. If the CP exists near the connection of the slot edge, then Point "I" was set to 200°; otherwise, "I" strain gauge would be ignored. The strain gauge layout plan for the YB1 slot was the same as that of NT2, except for measurement point I. Seven strain measuring points, namely, A, B, C, D, E, F, and G, were available for slot type T1, thus representing the location angles of –40°, –20°, 0°, 45°, 90°, 135°, and 180°. Figure 8 illustrates the strain gauge arrangements of the three typical holes.

Tolerances were ensured of mechanical prevention during indoor lab tests. Resistance strain indicators and a laptop computer were placed. The computers collected strain test data. For each specimen, a hole position in the top middle (B2) was selected for the strain measurements. To ensure an effective measurement, the strain gauges were positioned using an adhesion agent along the three principal stress directions at each point. Figure 9 illustrates detailed images of the experiment gauge layout compared with the real structure.

Then, the strain instruments were manipulated by the laptop used for measurement, wherein instrumental software was installed. The test gear should be reset to 0 when testing and inspecting the equipment. Thus, stress values could be transferred from the strain measurement and recognized as the experimental results compared with the numerical results drawn from this study.

3.3 Test result interpretation

Given the compression cases, 10, 20, 30, and 40 t forces were used, wherein the microcomputer control electron universal testing machine loaded the six specimens. Experimental strain data were collected from the measurement of location B2. Then, local von Mises (VM) stresses were calculated from the data using the built-in software. Table 3 summarizes the results.

The same transformation process was applied to the bending load cases. Forces of 1, 2, 3, and 4t were loaded on the stresses of the given specimens at Location B2. Table 4 displays the results.

The test results show that there is an obvious stress concentration phenomenon at the edge of the hole, and there is an obvious linear relationship between the load and the stress value at the edge of the hole. The greater the load, the greater the stress value at the edge of the hole. The stress distribution and stress concentration at the edge of the hole are only related to the hole type of the specimen and do not change with the change of the load.

Table 4: Stress measurement at the locations under bending conditions of B2 (unit: MPa)

|		A	B	C	D	E	F	G	H	I
NT2-CP0-FB0	10T	31.0	57.78	58.06	24.62	—	50.47	56.58	46.93	—
	20T	32.0	62.27	100.45	26.74	—	60.45	63.66	44.73	—
	30T	31.45	72.42	140.54	16.72	—	69.14	72.4	44.58	—
	40T	25.71	105.32	179.21	13.83	—	78.21	84.43	47.63	—
NT2-CP1-FB0	10T	—	13.56	36.49	27.32	11.43	—	9.22	17.67	16
	20T	—	38.83	73.79	43.28	7.11	—	14.18	24.37	20
	30T	—	62.57	109.55	52.43	8.11	—	17.34	31.7	25
	40T	—	86.65	146.39	61.9	9.88	—	23.38	38.46	29.3
NT2-CP0-FB1	10T	34.02	61.06	41.48	27.09	—	4.07	12.12	23.63	34.02
	20T	47.34	79.7	56.28	35.14	—	5.2	17.48	31.6	47.34
	30T	66.83	93.63	66.19	40.4	—	7.04	25.08	37.14	66.83
	40T	89.17	109.18	69.01	41.95	—	5.7	37.63	37.95	89.17
NT2-CP1-FB1	10T		26.1	12.46	6.63	3.45	11.24	7.53	8.99	6.53
	20T		45.91	25.03	14.61	5.77	17.81	14.56	17.93	8.96
	30T		57.12	32.24	20.46	7.83	21.5	17.16	24.04	8.97
	40T		66.4	38.74	24.81	9.37	24.14	18.97	32	8.38
T1-CP0-FB0	10T	28.81	64.05	70.69	23.6	—	4.76	6.84	8.62	—
	20T	56.63	119.72	92.81	46.89	—	8	15.12	18.42	—
	30T	79.13	173.63	133.2	65.31	—	7.97	24.61	27.07	—
	40T	103.26	218.93	172.19	83	—	15.28	33.9	39.49	—
YB1-CP0-FB0	10T	138.01	119.52	88.78	52.9	—	7.96	30.16	37.87	—
	20T	172.77	167.13	127.26	46.49	—	4.96	27.56	43.41	—
	30T	207.29	216.03	165.49	65.49	—	6.1	27.5	48.21	—
	40T	239.46	263.63	203.65	70.28	—	11.45	31.31	52.54	—

The maximum concentrated stress at the opening edge can be effectively reduced by adding a patch plate specimen.

4 FEM calculations

Given the test scenario and experiments, the finite element software ABAQUS was used to establish the finite element analysis model, as depicted in Figure 10. The element type of S4R is selected, and the mesh size is 5 mm × 5 mm, considering the mesh convergence. Constraints and loading cases of the simulation were based on test condition cases.

Two principal loading cases were exhibited. A vertical force of 40 t acted upon the top surface of the model, where the nodes of the upper lateral walls of the sample were unrestricted, and the nodes of the bottom plane were fixed at the displacement and rotation of nodes on the lower surface. Three-point bending loading was applied, wherein the vertical displacement U2 = 0 at the transverse connection was only fixed at the location of the two piers. As mentioned previously, the line vertical

(a)   (b)
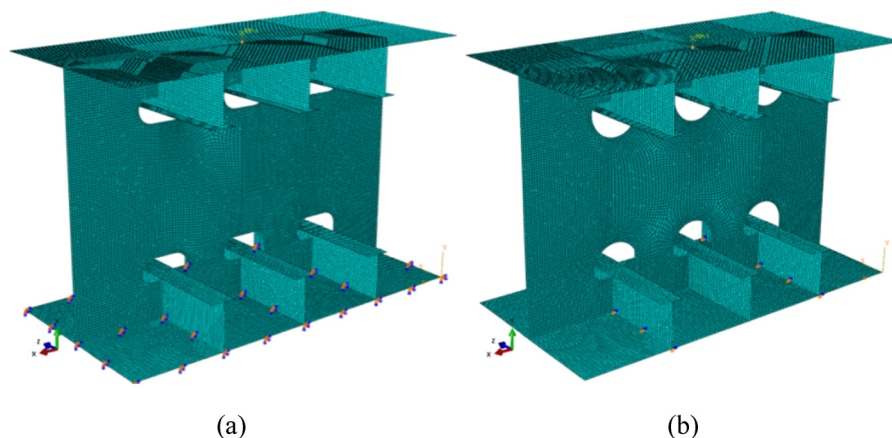
Figure 10: Finite element model of two cases: (a) compression loading case and (b) bending loading case.
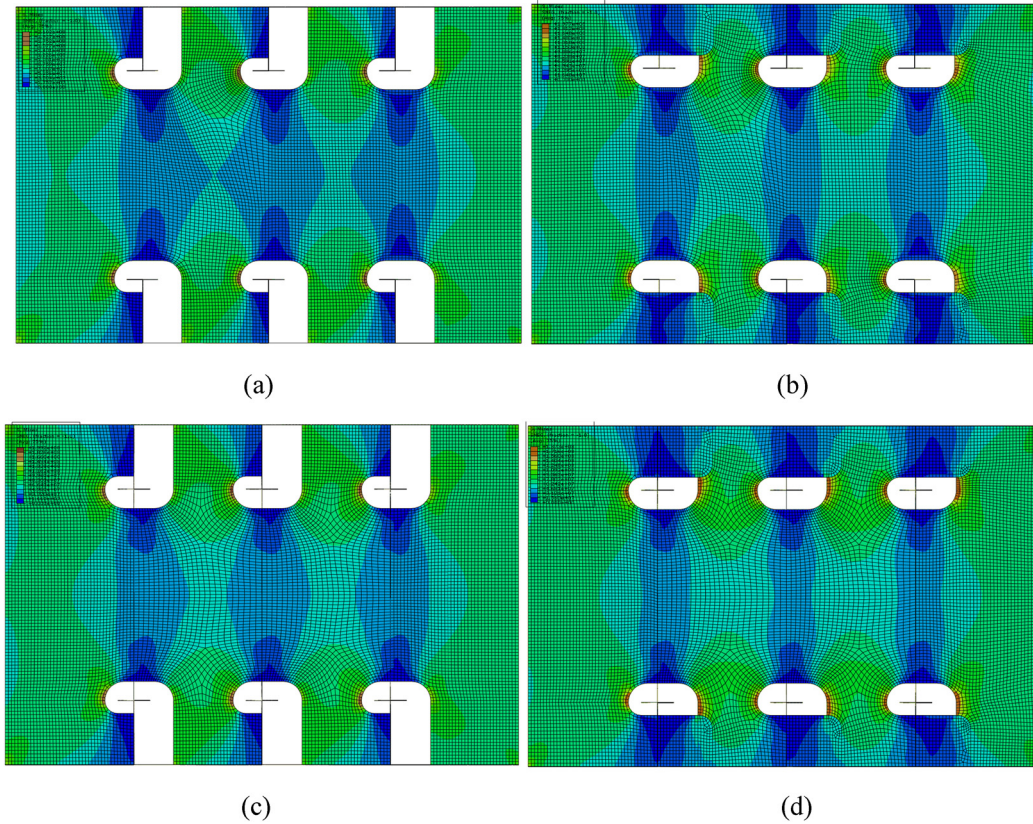
Figure 11: VM stress nephograms with FB and CP under compression: (a) NT2-CP0-FB0, (b) NT2-CP1-FB0, (c) NT2-CP0-FB1, and (d) NT2-CP1-FB1.

force of 4 t was applied to the positions of the middle line of the top surface, and the nodes of the upper and lower edge nodes were unrestricted in the vertical and horizontal directions. In both loading cases, the boundaries on the component edge were similar.

4.1 Results of compression force in the 40 t case

The application of a numerical compression force shows no remarkable contour differences between the six specimens, and the VM stresses are distributed non-uniformly. Figure 12 demonstrates the FEA results of the six kinds of components. Moreover, the results show the prominent specimen deformation of the bottom plates under hydrostatic pressures.

In the sample slot type without the CP NT2-CP1-FB0, the maximum VM stress (175.12 MPa) is 15.2% lower than that (206.5 MPa) of the original model of NT2-CP0-FB0. If we consider the combined effects of the web stiffener and CP, then the maximum stress is remarkably reduced by 21.3% to 162.55 MPa, as displayed in Figure 11.

The use of numerical calculations indicates that NT2 is superior to the other two types, namely, T1 (215.3 MPa) and YB1 (222.0 MPa), as presented in Figure 12. The peak stress results are also compared, wherein the influence of the CP and web stiffener can effectively reduce the peak stress under the compression case.

The peak VM stress of NT2-CP0 has decreased by 12.5% ratios from 206.5 to 180.61 MPa given the presence of a web stiffener. After analyzing the results, stress distribution has changed, wherein a new stress concentrated point with a value of 171.20 MPa is found at the connection between the web and web stiffeners. This stress concentrated point is an unfavorable location for a shell-to-bottom connection, considering high stresses that are inevitably produced in the welded joint.

4.2 Results of bending in the 4 t case.

The load is coupled through the reference point and the B2 hole that corresponds to the reinforcement on the upper surface of the specimen. Figure 13 presents the similar plotting of the bending cases, wherein the peak stress is 205.6 MPa for NT2-CP0-FB0. If a CP is added,
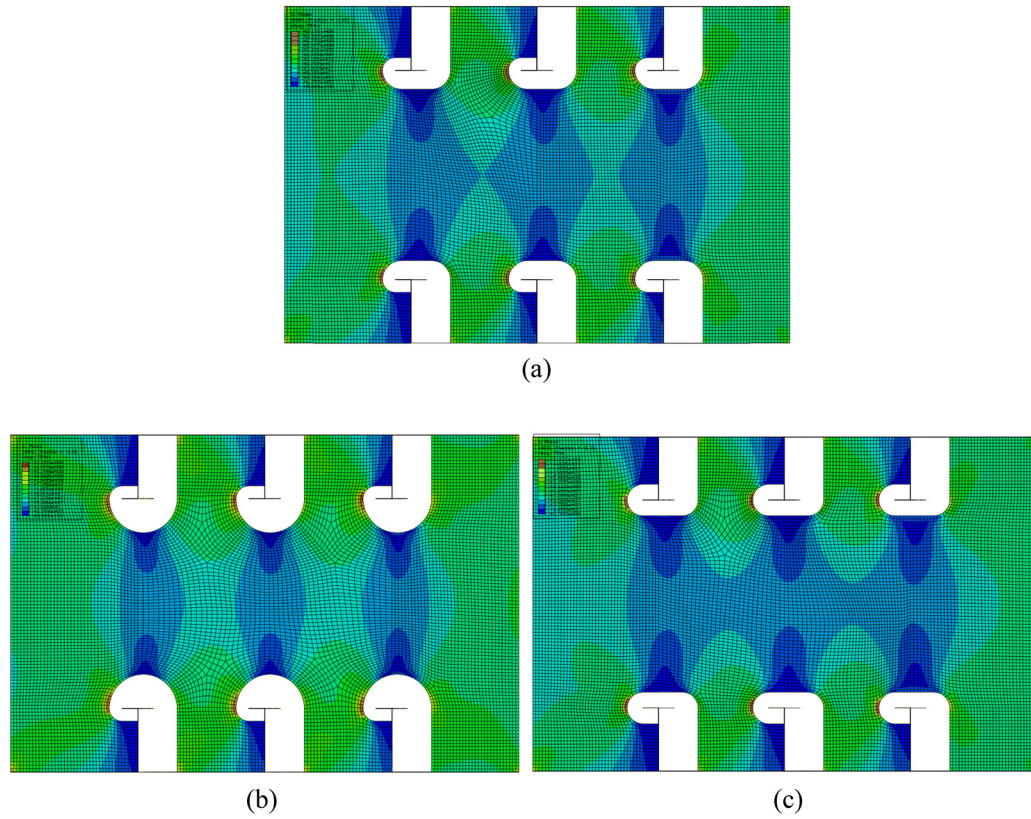
(a)

(b)

(c)

Figure 12: VM stress nephograms of slot type NT2, T1, and YB1 under 40 tons compression: (a) NT2-CP0-FB0, (b) T1-CP0-FB0, and (c) YB1-CP0-FB0.
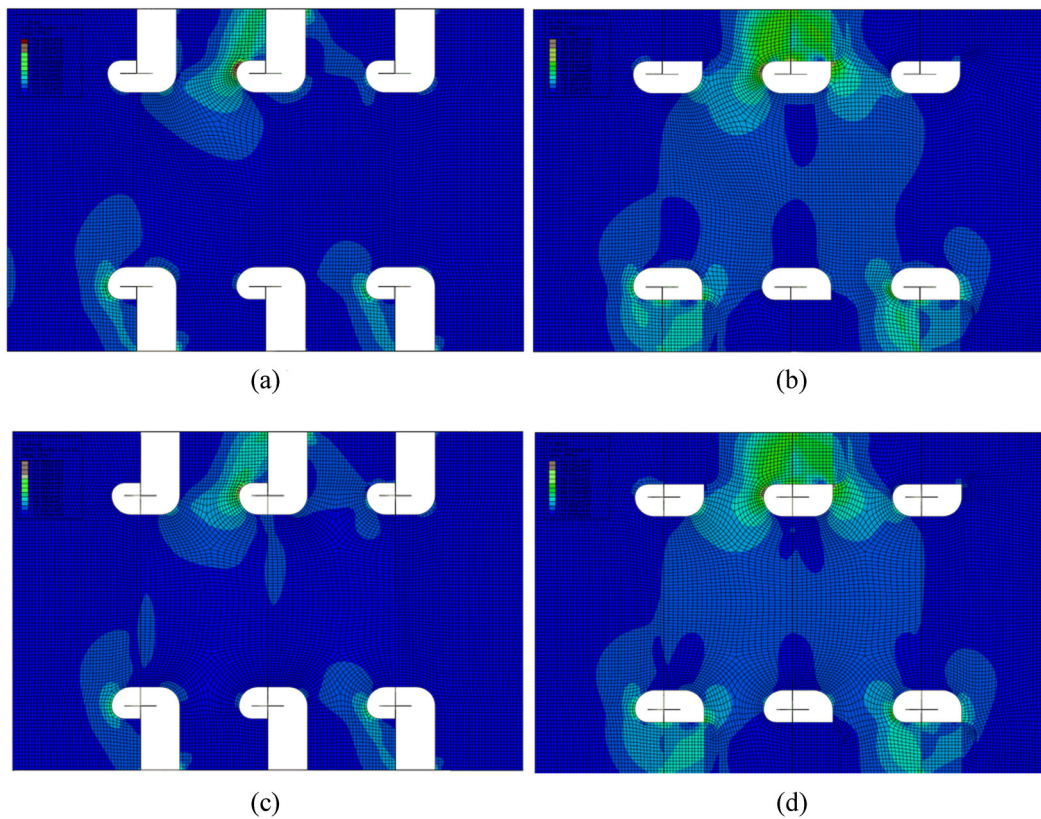

(a)

(b)

(c)

(d)

Figure 13: VM stress nephograms with FB and CP: (a) NT2-CP0-FB0, (b) NT2-CP1-FB0, (c) NT2-CP0-FB1, and (d) NT2-CP1-FB1.

then the value will decrease to 182.0 MPa. If the effect of the web stiffener is considered, then the stress will reduce by 42% to 118.8 MPa. If the combined effects of the CP and web stiffener are included, then the concentrated stress will be reduced to 71.3 MPa. Thus, the CP and web stiffener will help reduce the stress concentration.

As observed in the numerical results around the hole edge depicted in Figure 14, the structural stress of NT2 is the lowest at 198.3 MPa because the spherical shape of NT2 provides more space and transfers the stress more smoothly than the two other shapes.

5 Discussions

5.1 Uniform stress distributions versus angles

Figure 15 illustrates the comparison of the numerical and experimental concentrated stress results. The numerical and experimental results for each specimen of special loading cases are found to be similar. Research is provided

in the elasticity range. Stress becomes constant by dividing the normal stress, and the stress concentration factor (SCF) of the numerical and experimental results are nearly on the same line.

Figure 16 demonstrates the numerical results for each test specimen under the bending loading magnitude of 1–4 t. The numerical results are found to be consistent with the experimental results, wherein the SCF can be treated as a reference for the selected loading approaches of elasticity ranges.

After comparing the numerical and experimental results of compression and bending, local stress will be increased because of the weld point along the real connection. The numerical and experimental results for each specimen of special loading cases are found to be similar. Stress becomes constant by dividing the normal stress, and the SCFs of the numerical and experimental results are nearly on the same line. And the maximum stress concentration area is nearly 0°. The stress value of the test results is generally slightly higher than that of the finite element simulation results, mainly due to the welding deformation of some structures, so that the upper and lower plate surfaces are not completely flat and the pressure load acts on the transverse rib plate intensively through the base
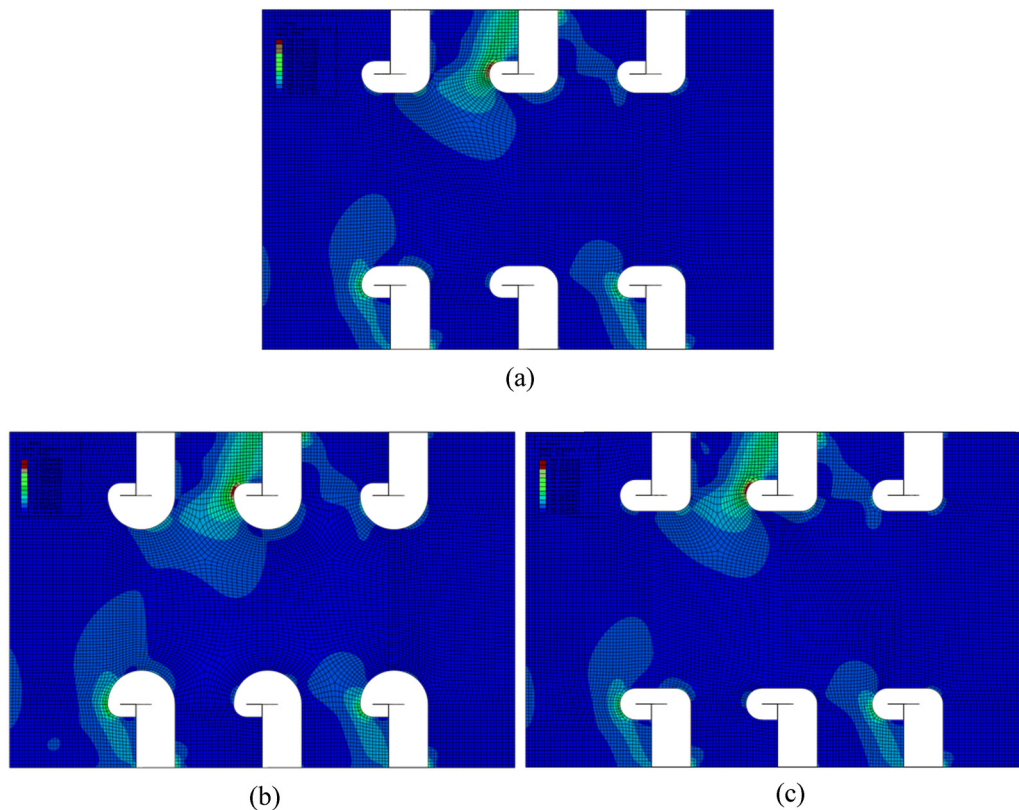

(a)

(b)

(c)

Figure 14: VM stress nephograms of slot types NT2, T1, and YB1 under 4T force: (a) NT2-CP0-FB0, (b) T1-CP0-FB0, and (c) YB1-CP0-FB0.
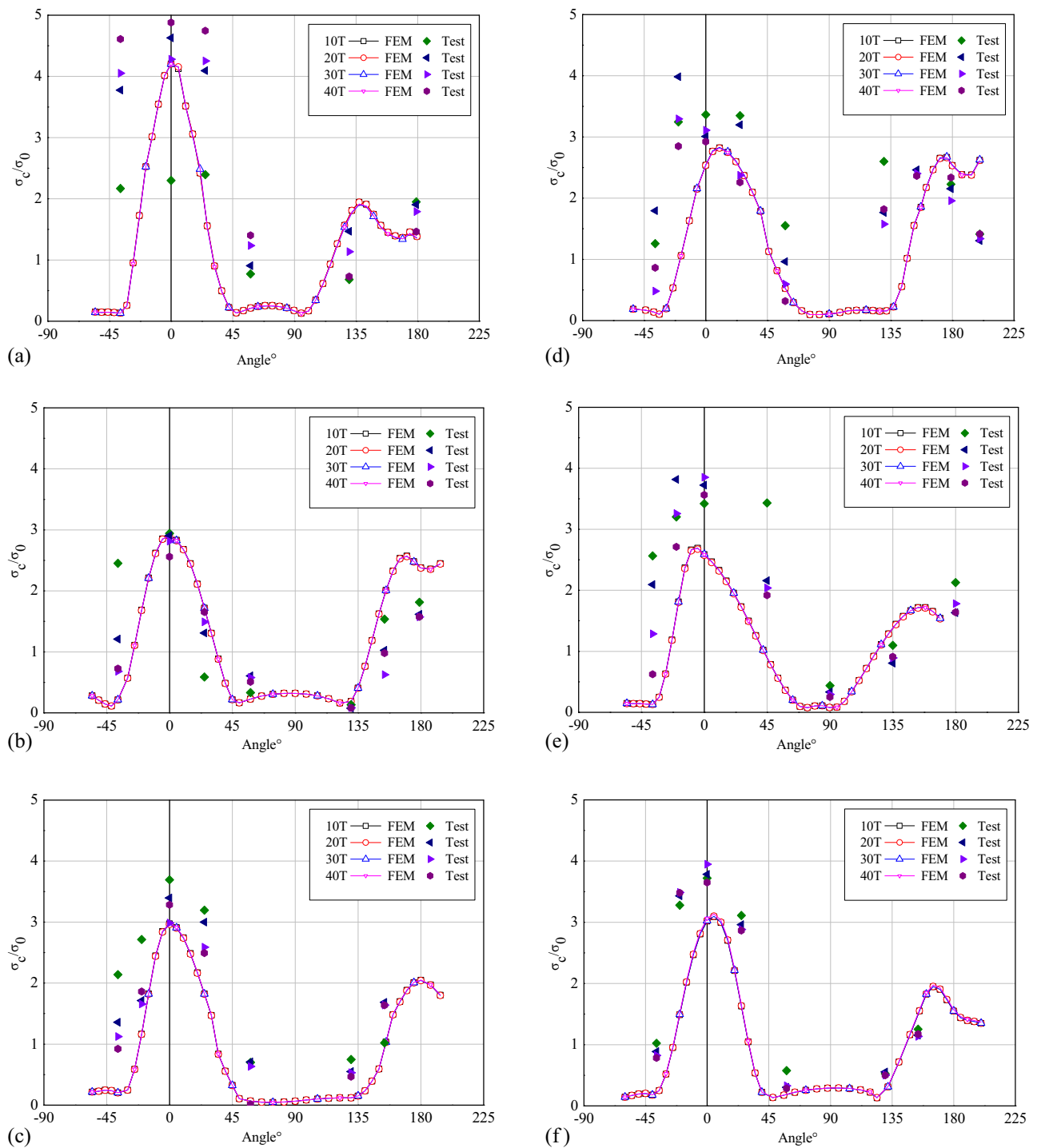
Figure 15: Compression uniform stress result of each specimen during the experiments: (a) uniform stress distributions of specimen NT2-CP0-FB0; (b) uniform stress distributions of specimen NT2-CP0-FB1; (c) uniform stress distributions of specimen NT2-CP1-FB0; (d) uniform stress distributions of specimen NT2-CP1-FB1; (e) uniform stress distributions of specimen T1-CP0-FB0; and (f) uniform stress distributions of specimen YB1-CP0-FB0.

plate, resulting in the measured hole edge stress value higher than the finite element calculation value. However, in some cases, there are obvious differences between the test results and the simulation results (Figures 15e and 16a). This is mainly related to component processing and stress concentration. Although several groups of tests have been carried out, the results have such consistency. However, this error does not affect the distribution of stress around the
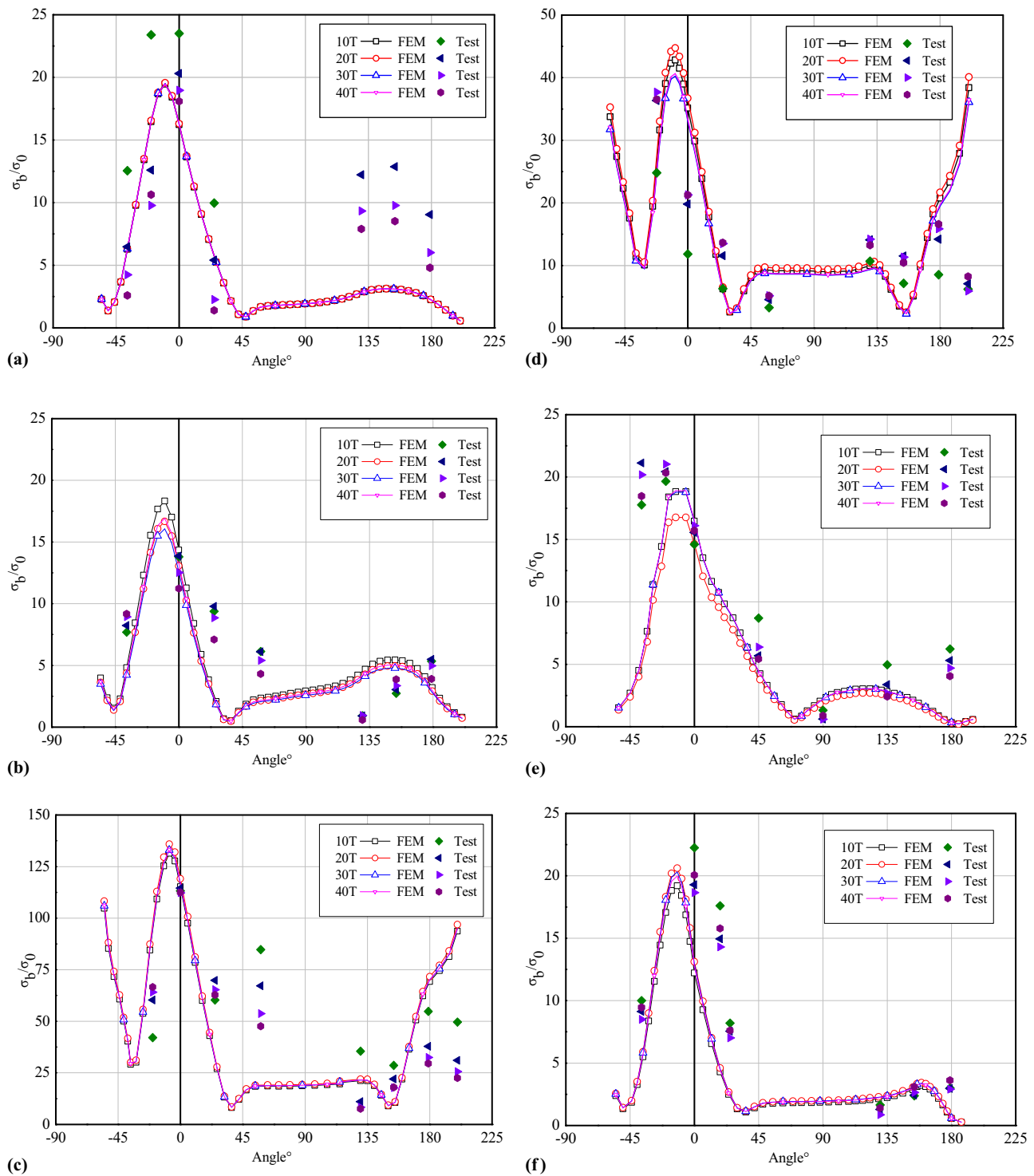
Figure 16: Bending uniform stress result of each specimen during the experiments: (a) uniform stress distributions of specimen NT2-CP0-FB0; (b) uniform stress distributions of specimen NT2-CP0-FB1; (c) uniform stress distributions of specimen NT2-CP1-FB0; (d) uniform stress distributions of specimen NT2-CP1-FB1; (e) uniform stress distributions of specimen T1-CP0-FB0; and (f) uniform stress distributions of specimen YB1-CP0-FB0.
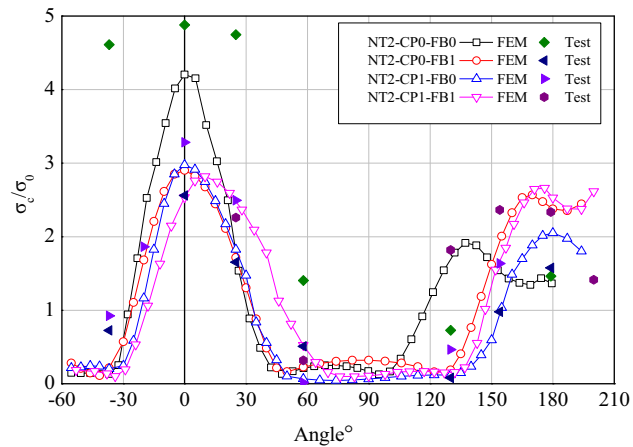
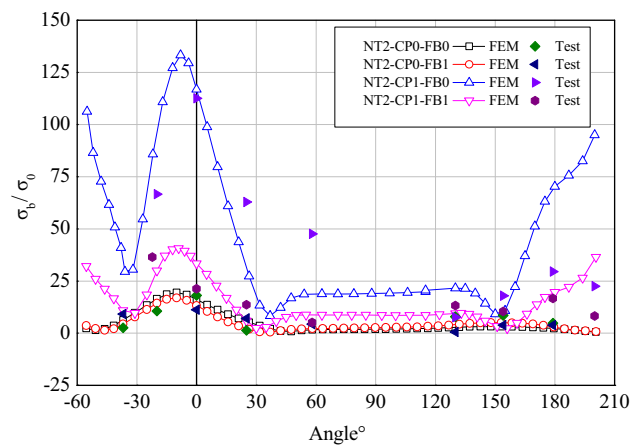**Figure 17:** Compression stress results of hole-type NT2 with (or without) CP and FB.

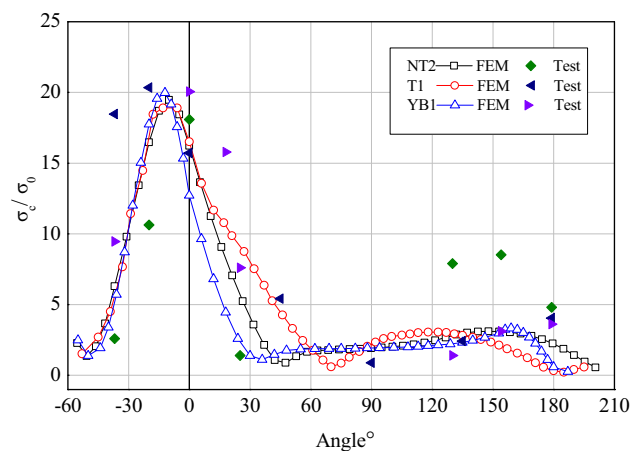**Figure 18:** Bending stress results of hole-type NT2 with (or without) CP and FB.

Figure 19: Compression stress results along slot types NT2, T1, and YB1.
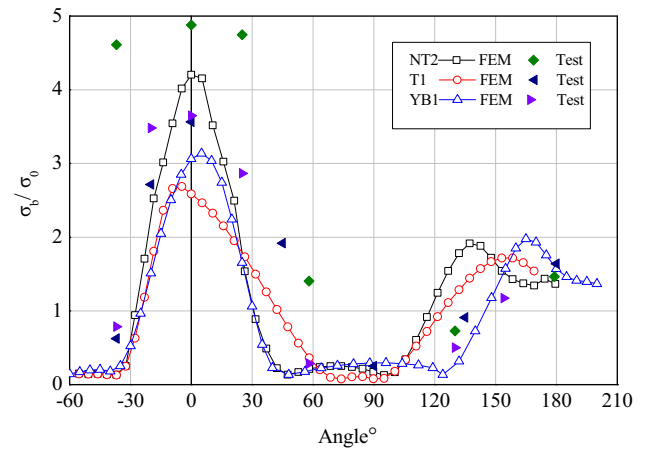

Figure 20: Bending stress results along slot types NT2, T1, and YB1.

hole and the presentation of stress concentration, and the error is acceptable to a certain extent.

5.2 Stress distributions of the NT2 specimen group under compression

Given that the calculations remain in the elasticity range, the 40 t compression load magnitude case has been selected to analyze the slot-type function and the influences of the CP and web stiffener. Similar uniformed stress concentration distributions have been established, as presented in Figure 17, and the CP will reduce the maximum stress value, which is the same function as the FB. Both attachment plates are used in the same specimen, which switches the maximum stress location to a new position.

5.3 Stress distributions of the NT2 specimen group under bending

Magnitude bending case results of 4 t load are selected and illustrated in Figure 18 to analyze the slot-type function and the influences of the CP and web stiffener.

The results show that the maximum concentrated stress will slightly decrease when the FB function is considered, as compared with the specimen without an attachment. If only the CP is included, then a new stress concentration occurs. As exhibited by the pink curve, adding a web stiffener will merge the peak stress and connection plate and cause the maximum stress to

increase, thereby indicating that the combined effects of the CP and FB (collaring arrangement) will benefit new building constructions.

5.4 Stress distributions of the different slot types under compression

For the different specimens of the slot types (i.e., NT2, T1, and YB1), numerical results under 40 t compression loading are used for analysis. Figure 19 summarizes the uniform stress of the numerical and experimental results. No significant difference exists between the stress distributions and maximum stress position because the compression forces are applied to the face panel rather than on the frames.

5.5 Stress distributions of the different slot types under bending

Based on the numerical results under the bending loading of 4 t from fatigue tests, Figure 20 illustrates the concentered stress distribution without considering the collaring arrangement. Two peak stresses exist at 0° and 150° around the hole edge from a single loading condition. At the 0° position of the T1 type, the maximum uniform stress is superior to the two other slot types, and several peak positions have effectively shared the loading. The second peak stress location shows that SCF = 2.0 at 135° of the NT specimen, SCF = 2.0 at 160° of YB1, and SCF = 1.6 at 150° of T1. T1 can balance the stress distributions.

6 Summary and conclusions

In this study, the resistance strain gauge technique was adopted for stress measurement, whereas the geometry features of various opening types were considered thoroughly through the FEM. The measurement and comparison of the stress distributions around the selected hole edge at the ship slot structures examined the characteristics of the slot types and effects of the CP and web stiffener. Numerical tools were utilized in this study to provide a continuous description of the stress distribution, and the experimental results were consistent with the numerical results. Based on observations and experimental and numerical analyses, the stress distributions

of the ship bottom construction were revealed, and a discussion of and recommendation for the bottom connection design and manufacture were presented. The relevant research results can effectively guide the opening optimization and strengthening design of hull structure, and also provide a verification basis for relevant theoretical analysis methods. The following conclusions and recommendations were drawn from this study.

1) By comparing the experimental and numerical results of the typical conditions, a large gap exists between the concentrated stresses of different cutout patterns. The stress distributions obtained from the experimental and numerical analyses provide valuable information in the design stage.

2) Stresses have been evaluated at Locations A–H for four specimens, namely, NT2-CP0-FB0, NT2-CP1-FB0, NT2-CP0-FB1, and NT2-CP1-FB1. Location C (or B and D) around the angle approximately between −30° and 20° is the critical section based on maximum stress criteria.

3) The comparison of the stress distributions of specimens NT2-CP0-FB0, T1-CP1-FB1, and YB1-CP1-FB1 indicates that NT2 is a reasonable slot type, wherein the stress distribution around the hole is smooth, and the peak stress of NT2-CP0-FB0 is the least among the slot types. Therefore, the cutout pattern must be considered on the basis of the different stress conditions at the actual structural position in the actual ship design process to increase the safety of the ship.

4) The comparison of the hole–edge stress distributions of the NT2 (-CP0-FB0, -CP0-FB1, -CP1-FB0, and -CP1-FB1) specimens under different reinforcing modes denotes that the stress concentration can be effectively reduced by adding CP and web stiffener. Consequently, adding a CP is beneficial for the safety of the structure. For the specimen under bending loads, a new concentrated location can be found if a CP is added. In this study, increased stress has not been predicted, and the authors agree that replacing the peak stress location is infeasible. Therefore, the CP and web stiffener must be used in designing or constructing the slot to reduce the stress concentration and optimize the strength.

Author contributions: All authors have accepted responsibility for the entire content of this manuscript and approved its submission.

Conflict of interest: The authors state there is no conflict of interest.

References

[1] Zhao C, Li J. Equilibrium selection under the Bayes-based strategy updating rules. Symmetry. 2020;12(5):739.

[2] Muskhelishvili NI. Some basic problems of the mathematical theory of elasticity. Math Gaz. 1964;48:445–7.

[3] Batista M. On the stress concentration around a hole in an infinite plate subject to a uniform load at infinity. Int J Mech Sci. 2011;53:254–61.

[4] Rao DKN, Babu MR, Reddy KRN, Sunil D. Stress around square and rectangular cutouts in symmetric laminates. Compos Struct. 2010;92:2845–59.

[5] Adi YA, Jayadi MI, Budiantoro A. Analytical approximation for the nonlinear dynamics of ERK activation in the presence of competitive inhibitor. Matrix Sci Math. 2020;4(1):10–3.

[6] Rezaeepazhand J, Jafari M. Stress concentration in metallic plates with special shaped cutout. Int J Mech Sci. 2010;52:96–102.

[7] Ukadgaonker VG, Rao DKN. A general solution for moments around holes in symmetric laminates. Compos Struct. 2000;49:41–54.

[8] Yang Y, Liu J, Cai C. Analytical solutions to stress concentration problem in plates containing rectangular hole under biaxial tensions. Acta Mech Solida. 2008;21:411–9.

[9] Wang Y, Wang H, Zhou B, Fu H. Multi-dimensional prediction method based on Bi-LSTMC for ship roll. Ocean Eng. 2021;242:110106–14.

[10] Long Q, Wu C, Wang X. A system of nonsmooth equations solver based upon subgradient method. Appl Math Comput. 2015;251:284–99.

[11] Sumi Y, Cervetto D, Das PK, Hakala M, Løeth R, Pegg N. Twophase finite element comparative study of a side structure of a middle size tanker. Mar Struct. 1996;9:151–79.

[12] Cheung MC, Slaughter SB. Innerbottom design problems in double-hull tankers. Mar Technol. 1998;97:512–4.

[13] Lotsberg I, Landet E. Fatigue capacity of side longitudinals in floating structures. Mar Struct. 2005;18:25–42.

[14] Huang X, Ma X, Li X, Fan J, Guo L, Yang H. Simultaneous realization of polarization conversion for reflected and transmitted waves with bi-functional metasurface. Sci Rep. 2022;11:12–3364.

[15] Wan Z, Xu B. Stress concentration factors of cutout for longitudinal. J Ship Mech. 2002;6:28–36.

[16] Fatigue and Fracture – ISSC 2003 – 15th International Ship and Offshore Structures Congress – III.2. ISSC 2003 – 15th International Ship and Offshore Structures Congress; 2003.

[17] Ship Structure Committee. Design guide for ship structural details; 1990.

[18] Zhang C, Abedini M. Development of P-I model for FRP composite retrofitted RC columns subjected to high strain rate loads using LBE function. Eng Struct. 2022;252:113580–631.